

**Pressure induced nonmonotonic evolution of superconductivity in 6R-TaS₂
with natural bulk van der Waals heterostructure**

Shaopeng Wang,^{1,2} Yuyan Han,¹ Sutao Sun,³ Shuyang Wang,¹ Chao An,⁴ Chunhua
Chen,¹ Lili Zhang,⁵ Yonghui Zhou,^{1,2,a)} Jian Zhou,^{3,a)} and Zhaorong Yang^{1,2,4,6,a)}

¹*Anhui Key Laboratory of Low-energy Quantum Materials and Devices, High Magnetic Field
Laboratory, HFIPS, Chinese Academy of Sciences, Hefei 230031, China*

²*Science Island Branch of Graduate School, University of Science and Technology of China, Hefei
230026, China*

³*National Laboratory of Solid State Microstructures and Department of Materials Science and
Engineering, Nanjing University, Nanjing 210093, China*

⁴*Institutes of Physical Science and Information Technology, Anhui University, Hefei 230601,
China*

⁵*Shanghai Synchrotron Radiation Facility, Shanghai Advanced Research Institute, Chinese
Academy of Sciences, Shanghai 201204, China*

⁶*Collaborative Innovation Center of Advanced Microstructures, Nanjing 210093, China*

^{a)}Corresponding authors: yhzhou@hmfll.ac.cn, zhoujian@nju.edu.cn and
zryang@issp.ac.cn

Abstract

The natural bulk van der Waals heterostructures compound $6R$ -TaS₂ consists of alternate stacking $1T$ - and $1H$ -TaS₂ monolayers, creating a unique system that incorporates charge-density-wave (CDW) order and superconductivity (SC) in distinct monolayers. Here, after confirming that the 2D nature of the lattice is preserved up to 8 GPa in $6R$ -TaS₂, we documented an unusual evolution of CDW and SC by conducting high-pressure electronic transport measurements. Upon compression, we observe a gradual suppression of CDW within the $1T$ -layers, while the SC exhibits a dome-shaped behavior that terminates at a critical pressure P_c around 2.9 GPa. By taking account of the fact that the substantial suppression of SC is concomitant with the complete collapse of CDW order at P_c , we argue that the $6R$ -TaS₂ behaves like a stack of Josephson junctions and thus the suppressed superconductivity can be attributed to the weakening of Josephson coupling associated with the presence of CDW fluctuations in the $1T$ -layers. Furthermore, the SC reversely enhances above P_c , implying the development of emergent superconductivity in the $1T$ -layers after the melting of T -layer CDW orders. These results show that the $6R$ -TaS₂ not only provides a promising platform to explore emergent phenomena but also serves as a model system to study the complex interactions between competing electronic states.

The advancements in the isolation and manipulation of atomically thin sheets of two-dimensional (2D) materials have paved the way for a new era of fundamental scientific research and technological innovation [1-4]. Nowadays, it has become feasible to independently fabricate distinct single layers possessing specific properties and subsequently assemble them into novel quantum materials known as van der Waals heterostructures (vdWHs). The constructed vdWHs not only combine the respective materials' functionalities but also imprint exotic properties through proximity interactions across the interface, leading to emergent phenomena such as Hofstadter butterfly states, tunable Mott insulators and topological superconductivity, etc [5-11].

Recently, there has been a growing interest in the exploration of emerging natural bulk vdWHs among transition-metal dichalcogenides [12-18]. Similar to the building blocks in 2D vdWHs, these bulk vdWHs are built as alternate stacking of octahedral (*T*) layers with charge-density-wave (CDW) order and trigonal-prismatic (*H*) layers with superconductivity (SC) and/or different CDW orders. To date, the bulk vdWHs are mainly concentrated on $4H_b$ - and $6R$ - TaX_2 ($X = \text{S}, \text{Se}$) [12-18]. For the $4H_b$ phase, taking $4H_b$ - TaS_2 as an example, the unit cell consists of four alternate stacking monolayers of $1T$ - TaS_2 and $1H$ - TaS_2 (half of $2H$ - TaS_2) [13]. The bulk $1T$ - TaS_2 is a Mott insulator [19] and candidate gapless quantum spin liquid [20], while the bulk $2H$ - TaS_2 is a superconductor known to also host a competing CDW order [21]. The natural combination of these two strongly correlated systems with proximity effect can generate fascinating physical phenomena like chiral SC, topological surface SC, and spontaneous vortices with a hidden magnetic phase [13, 16, 17]. As for the $6R$ phase, the typical compound $6R$ - TaS_2 is composed of six alternate stacking $1H$ - and $1T$ - TaS_2 layers in a unit cell, see Fig. 1(a). Recently, it has been reported that $6R$ - TaS_2 undergoes two CDW transitions from the

T-layer (nearly commensurate CDW transition at 320 K and commensurate CDW transition at 305 K) and enters the superconducting state from the adjacent *H*-layer below 2.7 K at ambient pressure [12]. The natural incorporation of CDW and SC in distinct layers makes 6*R*-TaS₂ stand out from the CDW materials, providing a unique platform to investigate the intriguing interplay between CDW and SC.

Pressure is proven to be an effective way of tuning the interlayer coupling and regulating the electronic properties in both artificial few-layer vdWHs and bulk TMDs [21-29]. In this work, we have investigated the pressure-induced evolution of the structural and electronic properties of 6*R*-TaS₂ single crystals, and unveil an unusual interplay between CDW and SC therein. With increasing pressure, the CDW order is destabilized monotonically, while the SC displays a dome-like behavior followed by a subsequent enhancement at higher pressures. Specifically, along with the complete collapse of CDW order at a critical pressure of around 2.9 GPa, the SC undergoes a simultaneous suppression. Since no structural phase transition or dimension crossover occurs throughout the pressure enhancement, we argue that the unusual evolution of SC can be well accounted for in a scenario of pressure tuning of Josephson coupling.

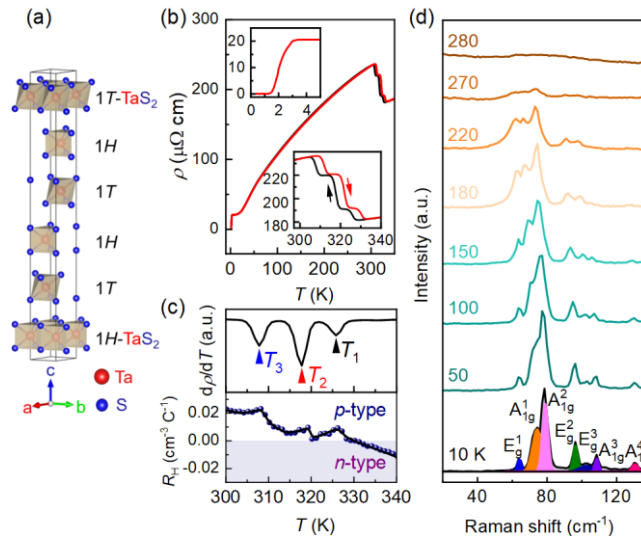


FIG. 1. (a) Schematic crystal structure of $6R$ -TaS₂. (b) Temperature-dependent resistivity curves at ambient pressure. Upper left inset: enlarged view around $T_c^{\text{onset}} \sim 2.8$ K (T_c^{onset} is determined by 90% of normal state resistivity). Lower right inset: thermal hysteresis across step-like resistivity upturns. (c) Temperature-dependent $d\rho/dT$ and Hall coefficient R_H between 300 and 340 K. The characteristic temperatures of three step-like upturns, are denoted by T_1 , T_2 , and T_3 , respectively. (d) Selected ambient-pressure Raman spectra from 10 to 280 K.

The synthesis and experimental details are given in the Supplemental Material [30]. Figure 1(b) shows the temperature-dependent resistivity $\rho(T)$ curves of $6R$ -TaS₂, which document a superconducting transition in the $1H$ -layer with $T_c^{\text{onset}} \sim 2.8$ K, and step-like upturns in a temperature range of about 30 K associated with the CDW transitions in the $1T$ -layer, consistent with the results of Achari *et al.* [12]. The step-like anomalies display clear hysteresis upon cooling and warming [see the inset of Fig. 1(b)]. As seen in Fig. 1(c), upon cooling across the CDW transitions, the anomalies manifest as dips in the corresponding derivative $d\rho/dT$ at 326 (T_1), 318 (T_2), and 308 K (T_3), while the Hall coefficient R_H changes sign from negative to positive followed by three peak-like anomalies at the corresponding temperatures. Note that Achari *et al.* have identified two CDW transitions in $6R$ -TaS₂ at 320 and 305 K, respectively, based on their electrical transport measurements [12]. The former was attributed to a transition from incommensurate to nearly commensurate (NC) CDW phase, and the latter was assigned to a NC- to commensurate (C) CDW transition [12]. Clearly, by alternately stacking the $1T$ - and $1H$ -layers, the low-temperature CCDW transition of the original $1T$ -layer is increased from 190 K in bulk to above room temperature in $6R$ -TaS₂ [25]. Meantime, the superconducting temperature in the $1H$ -layer is enhanced substantially compared to the value of 0.8 K in its bulk counterpart [43].

In addition to electrical transport measurements, the CDW state was also detected by Raman spectroscopy. Previous studies on the $1T$ -TaS₂ indicated that upon the CCDW transition, the zone-folding Raman modes manifest as a series of A_{1g} and E_g Raman modes below 140 cm⁻¹, which are the signature of the CCDW state [44, 45]. Figure 1(d) displays the temperature-dependent Raman spectra at ambient pressure and selected temperatures from 10 to 280 K. At 10 K, the zone-folding Raman modes exhibit four A_{1g} and three E_g modes. All the zone-folding modes are softened as temperature increases, and the CCDW feature can be observed until 270 K.

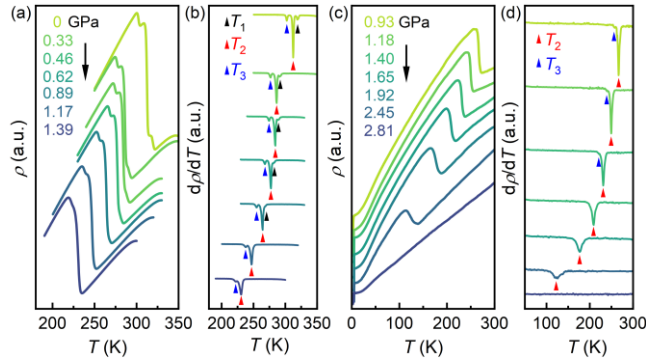


FIG. 2. Temperature-dependent resistivity of $6R$ -TaS₂ and its derivative $d\rho/dT$ in PCC [(a)-(b)] and DAC [(c)-(d)] setups. All the curves are offset for clarity (see the original data in Fig. S2).

After having characterized the sample quality, we first performed electronic measurements in a piston cylinder cell (PCC) setup, with Daphne 7373 as the pressure-transmitting medium (PTM) to examine the pressure-induced evolution of CDW. Figure 2(a) and 2(b) display the resistivity versus temperature $\rho(T)$ curves in the temperature range of 180 to 350 K and their derivative $d\rho/dT$ versus T within 1.39 GPa. At the starting pressure of 0 GPa, we observed three distinct step-like resistivity upturns which are consistent with the ambient pressure case shown in Fig.

1. During compression, the resistive upturn is progressively shifted to lower temperatures, indicating the suppression of CDW order. All three characteristic temperatures evolve independently without converging except that the amplitude of the resistivity anomaly around T_1 is suppressed more dramatically and cannot be discerned at 1.17 GPa.

To get full insight into the pressure effect on CDW orders and unveil the relationship between CDWs and superconductivity, we further conducted high-pressure electrical transport measurements with the PTM Daphne 7373 in a diamond anvil cell (DAC) setup. As shown in Fig. 2(c), at the starting pressure of 0.93 GPa, the resistivity displays an abrupt upturn at T_2 associated with the CDW transitions. The resistivity anomaly at T_3 can be discerned only in the $d\rho/dT$ curve. With increasing pressure, the resistivity upturn moves to lower temperatures, in agreement with the results in Fig. 2(a). At 2.81 GPa, the step-like feature suddenly disappears and cannot be detected in the $d\rho/dT$ curve either, which suggests the complete suppression of CDW orders. The suppression of the CDW around 2.81 GPa is further confirmed by the evolution of high-pressure Raman spectra at 80 K (see Fig. S5). It is noteworthy that 80 K is the lowest temperature explored in the measurement due to the strong signal from the background of Daphne 7373. As shown in Fig. S5, along with the suppression of the CDW, all the zone-folding modes continuously soften and are undetectable above 2.71 GPa.

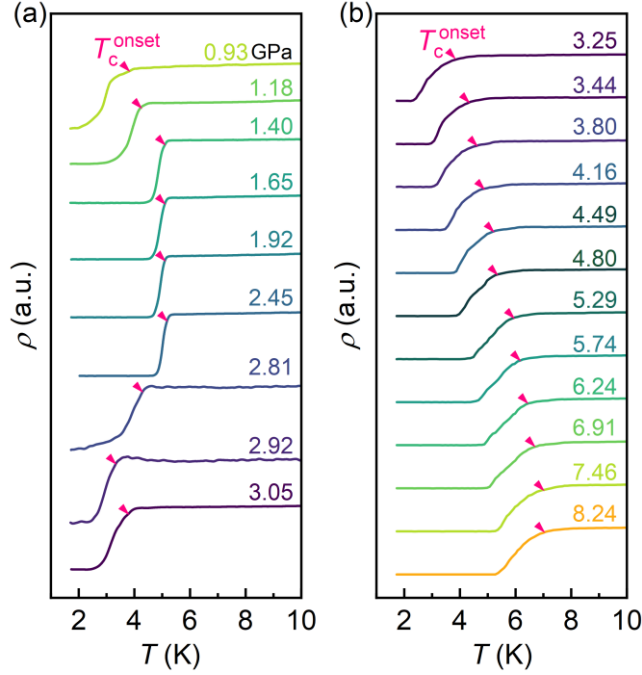


FIG. 3. (a)-(b) Low-temperature $\rho(T)$ curves in DAC setup. Pink solid triangle denotes the T_c^{onset} at each pressure. The curves are offset for clarity.

Figure 3 displays the pressure-induced evolution of the SC, illustrating a nonmonotonic variation of the superconducting transition temperature versus pressure. Compared with ambient pressure, the superconductivity gets a pronounced promotion at 0.93 GPa with $T_c^{\text{onset}} = 3.79$ K. The T_c^{onset} continuously increases with pressure, attaining approximately 5.16 K at 1.65 GPa. After that, the T_c^{onset} remains nearly constant. Interestingly, when reaching the pressure of CDW disappearance at 2.81 GPa, the T_c^{onset} decreases remarkably, accompanied by pronounced broadening of superconducting transition. Furthermore, at 3.05 GPa and above, the superconductivity gets another unexpected promotion. The T_c^{onset} keeps increasing and reaches the maximum values of 6.91 K at 8.24 GPa, the highest pressure in our transport measurement.

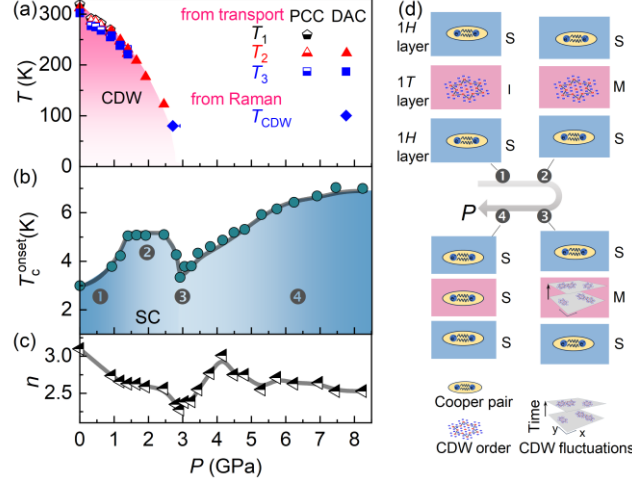


FIG. 4. Temperature-pressure phase diagram of $6R\text{-TaS}_2$. Pressure dependence of (a) CDW transition temperatures, (b) superconducting T_c^{onset} , and (c) parameter n from the analysis of the normal state resistivity. (d) Schematic illustration of pressure-tuned Josephson coupling in vdW $6R\text{-TaS}_2$ along with successive transformation of the 1T-layer from insulator (I) to metal (M) to metal with CDW fluctuations to superconductor.

Based on the above comprehensive high-pressure measurements, we constructed the temperature-pressure phase diagram of $6R\text{-TaS}_2$ as depicted in Fig. 4, which directly illustrates the evolutions of CDW and SC as well as their correlations. As can be seen, the T_{CDW} decreases monotonically to lower temperatures and extrapolates to zero at a critical pressure of around 2.9 GPa. Meantime, separated exactly by the same pressure, the $T_c^{\text{onset}}\text{-}P$ phase diagram reveals two distinct SC regions. The superconducting T_c^{onset} initially increases to 5.16 K upon compression up to 1.65 GPa then levels off followed by a sharp depression above 2.45 GPa, forming a dome-shaped superconducting state terminating exactly at 2.9 GPa. Above 2.9 GPa, the superconductivity experiences a resurgence, with T_c^{onset} eventually reaching the maximum of 6.91 K at 8.24 GPa. The presence of dome-shaped SC in response to external parameters like pressure is universal in the CDW materials. Associated with the competition between CDW and SC, the superconducting dome normally

develops right after the suppression of the CDW or displays a maximum at the critical pressure when the CDW collapses completely [28, 46, 47]. In some other cases, the maximum T_c is located in the vicinity of the quantum critical point, where the CDW fluctuations are responsible for the enhancement of SC [48-50]. In contrast, the dome in $6R\text{-TaS}_2$ ends up at the critical pressure corresponding to the disappearance of the CDW, which signals that the collapse of CDW is responsible for the synchronous suppression of SC.

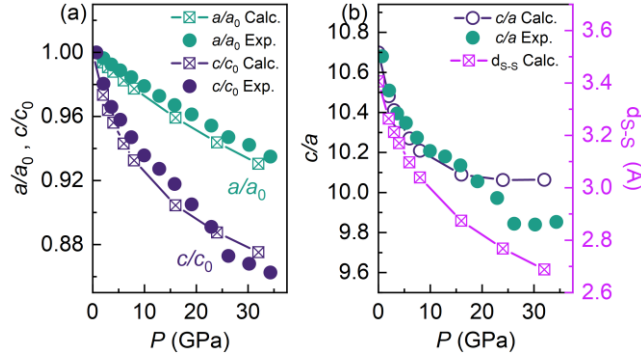


FIG. 5. (a) Experimental and calculated a/a_0 , c/c_0 ratios and (b) experimental and calculated c/a ratios and the calculated interlayer S-S distance (right axis) as a function of pressure. The a_0 and c_0 are the lattice constants of $6R\text{-TaS}_2$ at ambient pressure.

To clarify the unusual T_c evolution under pressure, we performed *in situ* high-pressure synchrotron XRD measurements on $6R\text{-TaS}_2$. As shown in Fig. S6, no structural phase transition is observed under compression up to 34.3 GPa. Both the lattice parameters c and a decrease monotonically, while c is compressed more pronounced because of the 2D nature of the lattice, which is also reflected in the pressure-dependent axial ratio c/a , see Fig. 5. Upon further compression above 25 GPa, c/a ratio becomes nearly constant, implying that the interlayer interactions become rather strong. Similar behavior in the c/a ratio has also been observed in pressurized CsV_3Sb_5 [51] and $4H_b\text{-TaSe}_2$ [14], and was attributed to the dimension

crossover from the quasi-2D to the 3D structure under pressure.

To gain more insight into the evolution of the crystal structure under high pressure, we performed the first-principles calculations on the high-pressure crystal structure of $6R$ -TaS₂. The structure information at various pressures is given in Table S1. The calculated a/a_0 , c/c_0 , and c/a are also plotted in Fig. 5(a) and 5(b). The evolution of the calculated parameters is well consistent with the experimental results below 8 GPa, but the c/c_0 and c/a deviate significantly from the experimental values above 20 GPa, possibly due to the nonhydrostatic pressure effect at higher pressure. Meantime, the c/a ratio rapidly decreases at low pressure, and the decay rate of c/a exhibits a crossover above 8 GPa. After applying pressure, sulfur atoms between adjacent H - and T -layers get close to each other along the c -axis. The distance d_{S-S} between the interlayer sulfur atoms is compressed from 3.55 Å at 0 GPa to 3.04 Å at 8 GPa and 2.87 Å at 16 GPa. Early work showed that the length of S-S bonds typically ranges between 1.8 and 3.0 Å [52], suggesting that below 8 GPa, $6R$ -TaS₂ maintains a vdW structure.

Without involving a structural transition, we will see that the unusual evolution of SC in pressurized $6R$ -TaS₂ is indeed rooted in the specific vdW 2D nature, which persists throughout the phase diagram in Fig. 4. At ambient pressure, the bulk $6R$ -TaS₂ is composed by alternate stacking of $1H$ - and $1T$ -TaS₂ layers, *i.e.*, alternating SC and CDW monolayers [12]. The superconductivity is not only determined by the pairing within the $1H$ -layer, but also more relied on the interlayer coupling that gives rise to a global phase coherence. This scenario is very similar to that in the high- T_c cuprate superconductors like Bi-2212, where the superconducting double layers are coupled by the Josephson effect, and the $6R$ -TaS₂ crystal is thus equivalent to a stack of superconductor-insulator-superconductor Josephson junctions [53, 54]. Taking into account the fact that the superconducting T_c in $2H$ -TaS₂, *i.e.*, the bulk counterpart of $1H$ -layer,

keeps continuous increasing below 8 GPa [28, 29, 55], we suggest that the pressure-induced nonmonotonic evolution of SC in $6R\text{-TaS}_2$ is mainly dominated by the unusual variation of the Josephson coupling as schematically illustrated in Fig. 4(d).

In the initial stage, as shown in panel 1 of Fig. 4(d), the Josephson coupling is mediated by tunneling of the Cooper pairs through the insulating barrier [53, 54, 56]. The increase of applied pressure leads to the decrease of the interlayer distance on one hand, and results in the suppression of CDW or insulating behavior in the middle $1T$ -layer on the other hand. Both are favorable to the enhancement of Josephson coupling and thereby improve the superconductivity.

The enhancing trend of superconductivity stops if the middle $1T$ -layer becomes metallic with increasing pressure [panel 2 in Fig. 4(d)]. In the case of SC-metal-SC junction, the Josephson coupling is accordingly established by the superconducting proximity effect rather than by the tunneling of Cooper pairs [56-61]. The proximity effect is characterized by inducing a superconducting order parameter in the metallic layer and weakening the superconductivity within a distance of the order of the coherence length in the SC layer [57, 59, 60]. The transformation of the coupling way by the proximity effect could be the main reason for the presence of the plateau between 1.65 and 2.45 GPa, otherwise, the T_c^{onset} should increase monotonically. In support of this speculation, as shown in Fig. S3, the resistivity along c -axis at 10 K drops by about an order of magnitude with increasing pressure from 0 to 1.62 GPa, above which it tends to be stable against the pressure.

From a microscopic point of view, the superconducting proximity effect is correlated to the Andreev reflection, *i.e.*, reflecting an incident electron as a hole in the metallic layer and transmitting a Cooper pair into the SC region correspondingly [56, 59, 60, 62]. Around 2.9 GPa, along

with the disappearance of the CDW order in the 1*T*-layer, the superconductivity displays a synchronous depression. Furthermore, the exponential parameter n , extracted from the fitting of $\rho(T)$ curves in the normal state with the empirical formula $\rho(T) = \rho_0 + AT^n$, also exhibits a dip feature around this critical pressure, see Fig. 4(c). The suppression of the parameter n can be viewed to be evidence of strong CDW fluctuations accompanied by the collapse of CDW order [21, 24, 48]. In the presence of CDW fluctuations, as illustrated in panel 3 of Fig. 4(d), it is plausible to expect that the transparency of the junction becomes lower because the CDW fluctuations give rise to critical scattering for the incident electron and hamper the realization of Andreev reflection, leading to the suppression of proximity effect [60].

Further increase of pressure beyond the first SC dome resulted in a subsequent resurgence of superconductivity, which can be attributed to the development of emergent superconductivity in the 1*T*-layers by referencing the studies of pressure-induced superconductivity in the bulk 1*T*-TaS₂ [24, 25]. Along with the presence of stronger superconductivity in the 1*T*-layers [see panel 4 of Fig. 4(d)], the scenario of stacking Josephson junctions is not applicable anymore, which should involve a dimension enhancement of the superconductivity.

In summary, by compressing the vdWHs compound that maintains its 2D vdW nature through the pressure enhancement in the T - P phase diagram, we documented an unusual interplay between SC and CDW. Associated with the modulation of inherent Josephson coupling under compression, the SC undergoes successive variations: initial increases, plateaus between 1.65 and 2.45 GPa, depresses around 2.9 GPa, and finally resurges at higher pressures. The Josephson coupling is highly suppressed at 2.9 GPa because of the presence of metallic conductivity and CDW fluctuations in the 1*T*-layers. Our findings of the CDW-fluctuation-induced suppressing of SC in

$6R\text{-TaS}_2$ may shed light on studying the interplay between competing electronic orders in the vdWHs.

ACKNOWLEDGMENTS

This work was supported by the National Key Research and Development Program of China (Grants No. 2023YFA1406102 and 2022YFA1602603), the National Natural Science Foundation of China (NSFC) (Grants No. 12374049, No. 12174395, No. 12204004, and No. 12004004), the Natural Science Foundation of Anhui Province (Grants No. 2308085MA16 and No. 2308085QA18). Yonghui Zhou was supported by the Youth Innovation Promotion Association CAS (Grant No. 2020443). A portion of this work was supported by the Basic Research Program of the Chinese Academy of Sciences Based on Major Scientific Infrastructures (No. JZHKYPT-2021-08). A portion of this work was performed on the Steady High Magnetic Field Facilities, High Magnetic Field Laboratory, CAS. The numerical calculations in this paper have been done on the computing facilities in the High Performance Computing Center (HPCC) of Nanjing University.

Reference

- [1] K.S. Novoselov, V.I. Fal'ko, L. Colombo, P.R. Gellert, M.G. Schwab and K. Kim, A roadmap for graphene, *Nature* **490**, 192 (2012). <https://doi.org/10.1038/nature11458>
- [2] Q.H. Wang, K. Kalantar-Zadeh, A. Kis, J.N. Coleman and M.S. Strano, Electronics and optoelectronics of two-dimensional transition metal dichalcogenides, *Nat. Nanotech.* **7**, 699 (2012). <https://doi.org/10.1038/nnano.2012.193>
- [3] M. Chhowalla, H.S. Shin, G. Eda, L.-J. Li, K.P. Loh and H. Zhang, The chemistry of two-dimensional layered transition metal dichalcogenide nanosheets, *Nat. Chem.* **5**, 263 (2013). <https://doi.org/10.1038/nchem.1589>
- [4] G. Fiori, F. Bonaccorso, G. Iannaccone, T. Palacios, D. Neumaier, A. Seabaugh, S.K. Banerjee and L. Colombo, Electronics based on two-dimensional materials, *Nat. Nanotech.* **9**, 768 (2014). <https://doi.org/10.1038/nnano.2014.207>
- [5] A.K. Geim and I.V. Grigorieva, Van der Waals heterostructures, *Nature* **499**, 419 (2013). <https://doi.org/10.1038/nature12385>
- [6] Y. Liu, N.O. Weiss, X.D. Duan, H.C. Cheng, Y. Huang and X.F. Duan, Van der Waals heterostructures and devices, *Nat. Rev. Mater.* **1**, 16042 (2016). <https://doi.org/10.1038/natrevmats.2016.42>
- [7] K.S. Novoselov, A. Mishchenko, A. Carvalho and A.H. Castro Neto, 2D materials and van der Waals heterostructures, *Science* **353**, aac9439 (2016). <https://doi.org/10.1126/science.aac9439>
- [8] S. Kezilebieke, M.N. Huda, V. Vaňo, M. Aapro, S.C. Ganguli, O.J. Silveira, S. Głodzik, A.S. Foster, T. Ojanen and P. Liljeroth, Topological superconductivity in a van der Waals heterostructure, *Nature* **588**, 424 (2020). <https://doi.org/10.1038/s41586-020-2989-y>
- [9] W.-M. Zhao, L. Zhu, Z. Nie, Q.-Y. Li, Q.-W. Wang, L.-G. Dou, J.-G. Hu, L. Xian, S. Meng and S.-C. Li, Moiré enhanced charge density wave state in twisted 1T-TiTe₂/1T-TiSe₂ heterostructures, *Nat. Mater.* **21**, 284 (2021). <https://doi.org/10.1038/s41563-021-01167-0>
- [10] B. Hunt, J.D. Sanchez-Yamagishi, A.F. Young, M. Yankowitz, B.J. LeRoy, K. Watanabe, T. Taniguchi, P. Moon, M. Koshino, P. Jarillo-Herrero and R.C. Ashoori, Massive Dirac Fermions and Hofstadter Butterfly in a van der Waals Heterostructure, *Science* **340**, 1427 (2013). <https://doi.org/10.1594/PANGAEA.808834>
- [11] G. Chen, L. Jiang, S. Wu, B. Lyu, H. Li, B.L. Chittari, K. Watanabe, T. Taniguchi, Z. Shi, J. Jung, Y. Zhang and F. Wang, Evidence of a gate-tunable Mott insulator in a

trilayer graphene moiré superlattice, *Nat. Phys.* **15**, 237 (2019).
<https://doi.org/10.1038/s41567-018-0387-2>

[12] A. Achari, J. Bekaert, V. Sreepal, A. Orekhov, P. Kumaravadivel, M. Kim, N. Gauquelin, P. Balakrishna Pillai, J. Verbeeck, F.M. Peeters, A.K. Geim, M.V. Milošević and R.R. Nair, Alternating Superconducting and Charge Density Wave Monolayers within Bulk $6R$ -TaS₂, *Nano Lett.* **22**, 6268 (2022).
<https://doi.org/10.1021/acs.nanolett.2c01851>

[13] A. Ribak, R. Majlin Skiff, M. Mograbi, P.K. Rout, M.H. Fischer, J. Ruhman, K. Chashka, Y. Dagan and A. Kanigel, Chiral superconductivity in the alternate stacking compound $4H_b$ -TaS₂, *Sci. Adv.* **6**, 9480 (2020). <https://doi.org/10.1126/sciadv.aax9480>

[14] L. Yan, C. Ding, M. Li, R. Tang, W. Chen, B. Liu, K. Bu, T. Huang, D. Dai, X. Jin, X. Yang, E. Cheng, N. Li, Q. Zhang, F. Liu, X. Liu, D. Zhang, S. Ma, Q. Tao, P. Zhu, S. Li, X. Lü, J. Sun, X. Wang and W. Yang, Modulating Charge-Density Wave Order and Superconductivity from Two Alternative Stacked Monolayers in a Bulk $4H_b$ -TaSe₂ Heterostructure via Pressure, *Nano Lett.* **23**, 2121 (2023).
<https://doi.org/10.1021/acs.nanolett.2c04385>

[15] S. Shen, T. Qin, J. Gao, C. Wen, J. Wang, W. Wang, J. Li, X. Luo, W. Lu, Y. Sun and S. Yan, Coexistence of Quasi-two-dimensional Superconductivity and Tunable Kondo Lattice in a van der Waals Superconductor, *Chin. Phys. Lett.* **39**, 077401 (2022).
<https://doi.org/10.1088/0256-307x/39/7/077401>

[16] E. Persky, A.V. Bjørli, I. Feldman, A. Almoalem, E. Altman, E. Berg, I. Kimchi, J. Ruhman, A. Kanigel and B. Kalisky, Magnetic memory and spontaneous vortices in a van der Waals superconductor, *Nature* **607**, 692 (2022).
<https://doi.org/10.1038/s41586-022-04855-2>

[17] A.K. Nayak, A. Steinbok, Y. Roet, J. Koo, G. Margalit, I. Feldman, A. Almoalem, A. Kanigel, G.A. Fiete, B. Yan, Y. Oreg, N. Avraham and H. Beidenkopf, Evidence of topological boundary modes with topological nodal-point superconductivity, *Nat. Phys.* **17**, 1413 (2021). <https://doi.org/10.1038/s41567-021-01376-z>

[18] J.J. Gao, J.G. Si, X. Luo, J. Yan, Z.Z. Jiang, W. Wang, Y.Y. Han, P. Tong, W.H. Song, X.B. Zhu, Q.J. Li, W.J. Lu and Y.P. Sun, Origin of the large magnetoresistance in the candidate chiral superconductor $4H_b$ -TaS₂, *Phys. Rev. B* **102**, 075138 (2020).
<https://doi.org/10.1103/PhysRevB.102.075138>

[19] P. Fazekas and E. Tosatti, Charge carrier localization in pure and doped $1T$ -TaS₂, *Phys. B+C* **99**, 183 (1980). [https://doi.org/10.1016/0378-4363\(80\)90229-6](https://doi.org/10.1016/0378-4363(80)90229-6)

[20] K.T. Law and P.A. Lee, $1T$ -TaS₂ as a quantum spin liquid, *Proc. Natl. Acad. Sci.*

U.S.A. **114**, 6996 (2017). <https://doi.org/10.1073/pnas.1706769114>

[21] S. Xu, J. Gao, Z. Liu, K. Chen, P. Yang, S. Tian, C. Gong, J. Sun, M. Xue, J. Gouchi, X. Luo, Y. Sun, Y. Uwatoko, H. Lei, B. Wang and J. Cheng, Effects of disorder and hydrostatic pressure on charge density wave and superconductivity in $2H\text{-TaS}_2$, *Phys. Rev. B* **103**, 224509 (2021). <https://doi.org/10.1103/PhysRevB.103.224509>

[22] J. Xia, J. Yan, Z. Wang, Y. He, Y. Gong, W. Chen, T.C. Sum, Z. Liu, P.M. Ajayan and Z. Shen, Strong coupling and pressure engineering in $\text{WSe}_2\text{-MoSe}_2$ heterobilayers, *Nat. Phys.* **17**, 92 (2020). <https://doi.org/10.1038/s41567-020-1005-7>

[23] T. Pandey, A.P. Nayak, J. Liu, S.T. Moran, J.-S. Kim, L.-J. Li, J.-F. Lin, D. Akinwande and A.K. Singh, Pressure-Induced Charge Transfer Doping of Monolayer Graphene/ MoS_2 Heterostructure, *Small* **12**, 4063 (2016). <https://doi.org/10.1002/sml.201600808>

[24] B. Wang, Y. Liu, X. Luo, K. Ishigaki, K. Matsubayashi, W. Lu, Y. Sun, J. Cheng and Y. Uwatoko, Universal phase diagram of superconductivity and charge density wave versus high hydrostatic pressure in pure and Se-doped $1T\text{-TaS}_2$, *Phys. Rev. B* **97**, 220504 (2018). <https://doi.org/10.1103/PhysRevB.97.220504>

[25] B. Sipoš, A.F. Kusmartseva, A. Akrap, H. Berger, L. Forró and E. Tutiš, From Mott state to superconductivity in $1T\text{-TaS}_2$, *Nat. Mater.* **7**, 960 (2008). <https://doi.org/10.1038/nmat2318>

[26] Q. Dong, J. Pan, S. Li, Y. Fang, T. Lin, S. Liu, B. Liu, Q. Li, F. Huang and B. Liu, Record-High Superconductivity in Transition Metal Dichalcogenides Emerged in Compressed $2H\text{-TaS}_2$, *Adv. Mater.* **34**, 2103168 (2022). <https://doi.org/10.1002/adma.202103168>

[27] Q. Dong, Q. Li, S. Li, X. Shi, S. Niu, S. Liu, R. Liu, B. Liu, X. Luo, J. Si, W. Lu, N. Hao, Y. Sun and B. Liu, Structural phase transition and superconductivity hierarchy in $1T\text{-TaS}_2$ under pressure up to 100 GPa, *npj Quantum Mater.* **6**, 20 (2021). <https://doi.org/10.1038/s41535-021-00320-x>

[28] Y. Kvashnin, D. VanGennep, M. Mito, S.A. Medvedev, R. Thiyagarajan, O. Karis, A.N. Vasiliev, O. Eriksson and M. Abdel-Hafiez, Coexistence of Superconductivity and Charge Density Waves in Tantalum Disulfide: Experiment and Theory, *Phys. Rev. Lett.* **125**, 186401 (2020). <https://doi.org/10.1103/PhysRevLett.125.186401>

[29] D.C. Freitas, P. Rodière, M.R. Osorio, E. Navarro-Moratalla, N.M. Nemes, V.G. Tissen, L. Cario, E. Coronado, M. García-Hernández, S. Vieira, M. Núñez-Regueiro and H. Suderow, Strong enhancement of superconductivity at high pressures within the charge-density-wave states of $2H\text{-TaS}_2$ and $2H\text{-TaSe}_2$, *Phys. Rev. B* **93**, 184512 (2016).

<https://doi.org/10.1103/PhysRevB.93.184512>

[30] See Supplemental Material [<http://link.aps.org/supplemental/>] for experimental and first-principles calculations details and the supporting results, which includes Refs. [14, 31-42].

[31] Y. Ding, L. Yang, C.-C. Chen, H.-S. Kim, M.J. Han, W. Luo, Z. Feng, M. Upton, D. Casa, J. Kim, T. Gog, Z. Zeng, G. Cao, H.-K. Mao and M. van Veenendaal, Pressure-Induced Confined Metal from the Mott Insulator $\text{Sr}_3\text{Ir}_2\text{O}_7$, *Phys. Rev. Lett.* **116**, 216402 (2016). <https://doi.org/10.1103/PhysRevLett.116.216402>

[32] X.-C. Pan, X. Chen, H. Liu, Y. Feng, Z. Wei, Y. Zhou, Z. Chi, L. Pi, F. Yen, F. Song, X. Wan, Z. Yang, B. Wang, G. Wang and Y. Zhang, Pressure-driven dome-shaped superconductivity and electronic structural evolution in tungsten ditelluride, *Nat. Commun.* **6**, 7805 (2015). <https://doi.org/10.1038/ncomms8805>

[33] C. Prescher and V.B. Prakapenka, DIOPTAS: a program for reduction of two-dimensional X-ray diffraction data and data exploration, *High Pressure Res.* **35**, 223 (2015). <https://doi.org/10.1080/08957959.2015.1059835>

[34] B.A. Hunter, RIETICA—A Visual Rietveld Program, International Union of Crystallography Commission on Powder Diffraction, Newsletter No. 20 (1998), www.rietica.org.

[35] H.-K. Mao, J. Xu and P.M. Bell, Calibration of the ruby pressure gauge to 800 kbar under quasi-hydrostatic conditions, *J. Geophys. Res.* **91**, 4673 (1986). <https://doi.org/10.1029/JB091iB05p04673>

[36] A. Eiling and J.S. Schilling, Pressure and temperature dependence of electrical resistivity of Pb and Sn from 1-300K and 0-10 GPa-use as continuous resistive pressure monitor accurate over wide temperature range; superconductivity under pressure in Pb, Sn and In, *J. Phys. F* **11**, 623 (1981). <https://doi.org/10.1088/0305-4608/11/3/010>

[37] K. G. and J. Furthmüller, Efficiency of ab-initio total energy calculations for metals and semiconductors using a plane-wave basis set, *Comp. Mater. Sci.* **6**, 15 (1996). [https://doi.org/10.1016/0927-0256\(96\)00008-0](https://doi.org/10.1016/0927-0256(96)00008-0)

[38] G. Kresse and J. Furthmüller, Efficient iterative schemes for ab initio total-energy calculations using a plane-wave basis set, *Phys. Rev. B* **59**, 1758 (1996). <https://doi.org/10.1103/PhysRevB.54.11169>

[39] P.E. Blöchl, Projector augmented-wave method, *Phys. Rev. B* **50**, 17953 (1994). <https://doi.org/10.1103/PhysRevB.50.17953>

[40] G. Kresse and D. Joubert, From ultrasoft pseudopotentials to the projector

augmented-wave method, *Phys. Rev. B* **59**, 1758 (1999).
<https://doi.org/10.1103/PhysRevB.59.1758>

[41] J.P. Perdew, K. Burke and M. Ernzerhof, Generalized Gradient Approximation Made Simple, *Phys. Rev. Lett.* **77**, 3865 (1996).
<https://doi.org/10.1103/PhysRevLett.77.3865>

[42] F. Jellinek, The system tantalum - sulfur, *J. Less-Common Met.* **4**, 9 (1962).
[https://doi.org/10.1016/0022-5088\(62\)90053-X](https://doi.org/10.1016/0022-5088(62)90053-X)

[43] K.E. Wagner, E. Morosan, Y.S. Hor, J. Tao, Y. Zhu, T. Sanders, T.M. McQueen, H.W. Zandbergen, A.J. Williams, D.V. West and R.J. Cava, Tuning the charge density wave and superconductivity in Cu_xTaS_2 , *Phys. Rev. B* **78**, 104520 (2008).
<https://doi.org/10.1103/PhysRevB.78.104520>

[44] O.R. Albertini, R. Zhao, R.L. McCann, S. Feng, M. Terrones, J.K. Freericks, J.A. Robinson and A.Y. Liu, Zone-center phonons of bulk, few-layer, and monolayer $1T\text{-TaS}_2$: Detection of commensurate charge density wave phase through Raman scattering, *Phys. Rev. B* **93**, 214109 (2016).
<https://doi.org/10.1103/PhysRevB.93.214109>

[45] S. Djurdjić Mijin, A. Baum, J. Bekaert, A. Šolajić, J. Pešić, Y. Liu, G. He, M.V. Milošević, C. Petrovic, Z.V. Popović, R. Hackl and N. Lazarević, Probing charge density wave phases and the Mott transition in $1T\text{-TaS}_2$ by inelastic light scattering, *Phys. Rev. B* **103**, 245133 (2021). <https://doi.org/10.1103/PhysRevB.103.245133>

[46] Z.Y. Liu, J. Li, J.F. Zhang, J. Li, P.T. Yang, S. Zhang, G.F. Chen, Y. Uwatoko, H.X. Yang, Y. Sui, K. Liu and J.G. Cheng, Quasi-one-dimensional superconductivity in the pressurized charge-density-wave conductor HfTe_3 , *npj Quantum Mater.* **6**, 90 (2021).
<https://doi.org/10.1038/s41535-021-00393-8>

[47] B. Shen, F. Du, R. Li, A. Thamizhavel, M. Smidman, Z.Y. Nie, S.S. Luo, T. Le, Z. Hossain and H.Q. Yuan, Evolution of charge density wave order and superconductivity under pressure in LaPt_2Si_2 , *Phys. Rev. B* **101**, 144501 (2020).
<https://doi.org/10.1103/PhysRevB.101.144501>

[48] A.F. Kusmartseva, B. Sipos, H. Berger, L. Forró and E. Tutiš, Pressure Induced Superconductivity in Pristine $1T\text{-TiSe}_2$, *Phys. Rev. Lett.* **103**, 236401 (2009).
<https://doi.org/10.1103/PhysRevLett.103.236401>

[49] M. Monteverde, J. Lorenzana, P. Monceau and M. Núñez-Regueiro, Quantum critical point and superconducting dome in the pressure phase diagram of o-TaS_3 , *Phys. Rev. B* **88**, 180504(R) (2013). <https://doi.org/10.1103/PhysRevB.88.180504>

[50] H. Kim, J.H. Shim, S. Kim, J.-H. Park, K. Kim and B.I. Min, Unusual Pressure-

Induced Quantum Phase Transition from Superconducting to Charge-Density Wave State in Rare-Earth-Based Heusler LuPd₂In Compound, *Phys. Rev. Lett.* **125**, 157001 (2020). <https://doi.org/10.1103/PhysRevLett.125.157001>

[51] F. Yu, X. Zhu, X. Wen, Z. Gui, Z. Li, Y. Han, T. Wu, Z. Wang, Z. Xiang, Z. Qiao, J. Ying and X. Chen, Pressure-Induced Dimensional Crossover in a Kagome Superconductor, *Phys. Rev. Lett.* **128**, 077001 (2022). <https://doi.org/10.1103/PhysRevLett.128.077001>

[52] R. Steudel, Properties of Sulfur-Sulfur Bonds, *Angew. Chem. Int. Ed.* **14**, 655 (2003). <https://doi.org/10.1002/anie.197506551>

[53] R. Kleiner and P. Müller, Intrinsic Josephson effects in high- T_c superconductors, *Phys. Rev. B* **49**, 1327 (1994). <https://doi.org/10.1103/PhysRevB.49.1327>

[54] R. Kleiner, F. Steinmeyer, G. Kunkel and P. Müller, Intrinsic Josephson effects in Bi₂Sr₂CaCu₂O₈ single crystals, *Phys. Rev. Lett.* **68**, 2394 (1992). <https://doi.org/10.1103/PhysRevLett.68.2394>

[55] X.-M. Zhao, K. Zhang, Z.-Y. Cao, Z.-W. Zhao, V.V. Struzhkin, A.F. Goncharov, H.-K. Wang, A.G. Gavriliuk, H.-K. Mao and X.-J. Chen, Pressure tuning of the charge density wave and superconductivity in 2H-TaS₂, *Phys. Rev. B* **101**, 134506 (2020). <https://doi.org/10.1103/PhysRevB.101.134506>

[56] G.-H. Lee and H.-J. Lee, Proximity coupling in superconductor-graphene heterostructures, *Rep. Prog. Phys.* **81**, 056502 (2018). <https://doi.org/10.1088/1361-6633/aaafe1>

[57] K.K. Likharev, Superconducting weak links, *Rev. Mod. Phys.* **51**, 101 (1979). <https://doi.org/10.1103/RevModPhys.51.101>

[58] X. Montiel and A.I. Buzdin, On the theory of the proximity effect in atomic scale superconducting/normal metal multilayered structures, *Supercond. Sci. Technol.* **26**, 085011 (2013). <https://doi.org/10.1088/0953-2048/26/8/085011>

[59] F. Tafuri and J.R. Kirtley, Weak links in high critical temperature superconductors, *Rep. Prog. Phys.* **68**, 2573 (2005). <https://doi.org/10.1088/0034-4885/68/11/r03>

[60] O.T. Valls, M. Bryan and I. Žutić, Superconducting proximity effects in metals with a repulsive pairing interaction, *Phys. Rev. B* **82**, 134534 (2010). <https://doi.org/10.1103/PhysRevB.82.134534>

[61] C.J. Lambert and R. Raimondi, Phase-coherent transport in hybrid superconducting nanostructures, *J. Phys.: Condens. Matter* **10**, 901 (1998). <https://doi.org/10.1088/0953-8984/10/5/003>

[62] H. Courtois, P. Gandit and B. Pannetier, Proximity-induced superconductivity in a narrow metallic wire, *Phys. Rev. B* **52**, 1162 (1995).
<https://doi.org/10.1103/PhysRevB.52.1162>